

Single-crystal X-ray analysis<sup>11</sup> of the orange crystals that initially form from the slow evaporation of a THF solution confirms the presence of *meso*-eLTTP in a cradle geometry that is bridging and chelating a Co-Co dimer. An ORTEP plot of *meso*-Co<sub>2</sub>(μ-CO)<sub>2</sub>(CO)<sub>2</sub>(eLTTP) (**1**) is shown in Figure 1, with important bond distances and angles. The molecule lies on a crystallographic mirror plane that passes through the bridging carbonyl ligands and the central methylene group of the eLTTP ligand. The Co-Co bond length of 2.513 (4) Å is typical for a Co-Co single bond.<sup>12</sup> The local coordination geometry about the cobalt atoms (ignoring the Co-Co bond) is a distorted trigonal bipyramid with the equatorial plane defined by P1, C1 and C2. This can be contrasted with the structure of the starting material Co<sub>2</sub>(μ-CO)<sub>2</sub>(CO)<sub>2</sub>-(norbadiene), which has a square-pyramidal coordination geometry.<sup>12a</sup> The *meso*-eLTTP ligand symmetrically bridges and chelates both cobalt centers with the two five-membered chelate rings eclipsed and oriented syn to one another. Due to the crystallographic mirror plane, all four phosphorus atoms lie in the same plane. The distorted trigonal-bipyramidal coordination environment about the cobalt centers results from the predicted coordination requirements of the eLTTP ligand.

The cradle-like geometry imposed by *meso*-eLTTP about the two cobalt centers is clearly seen in Figure 1. The fusing of a

bis(phosphino)methane bridging unit with two syn-oriented five-membered chelate rings creates a binucleating framework that is unique among polydentate ligand systems. Several differences between **1** and traditional cradle M<sub>2</sub>(R<sub>2</sub>PCH<sub>2</sub>PR<sub>2</sub>)<sub>2</sub> complexes exist, the most obvious being the presence of only a single P-CH<sub>2</sub>-P bridge. Another difference is that cisoidal P-M-P angles in cradle complexes range between 98 and 138°, with most values clustered around 109°. In **1**, however, the five-membered chelate rings rigorously enforce the considerable smaller angle of 85°. Perhaps the most important advantage for our complex is the *ligand-enforced* cradle geometry in *meso*-LTTP. Cradle complexes based on R<sub>2</sub>PCH<sub>2</sub>PR<sub>2</sub> ligands can often readily reconvert to A-frame orientations,<sup>3b,3d</sup> while a *meso*-M<sub>2</sub>(eLTTP) dimer, on the other hand, *cannot* rearrange this way.

The ability of eLTTP to enforce this new bimetallic cradle coordination geometry in Co-Co-bonded dimers opens a new synthetic route to cradle complexes of other metals. By enforcing this cradle geometry on the dimer, we anticipate the ability to access and extend the unique reactivities observed in other cradle dimer systems.<sup>3a,b,d,5</sup> We are exploring the reactivity of this new eLTTP-based bimetallic complex and will report these studies in the near future.

**Acknowledgment.** We thank the National Science Foundation (Grant CHE-86-13089) for supporting this research.

**Supplementary Material Available:** A complete ORTEP plot of **1** excluding H atoms and tables of crystal and structure refinement parameters, positional parameters, full bond distances and angles, and anisotropic thermal parameters (7 pages); a listing of observed and calculated structure factors (4 pages). Ordering information is given on any current masthead page.

Department of Chemistry  
Louisiana State University  
Baton Rouge, Louisiana 70803-1804

Scott A. Laneman  
Frank R. Fronczek  
George G. Stanley\*

Received January 17, 1989

- (11) **1** crystallizes in the orthorhombic space group *Pnma*, with the following unit cell parameters: *a* = 12.086 (4) Å, *b* = 21.645 (3) Å, *c* = 14.345 (2) Å, *V* = 3752 (2) Å<sup>3</sup>, *Z* = 4. Data were collected on an Enraf-Nonius CAD4 diffractometer with Mo Kα radiation, and an empirical absorption correction was performed. The structure was solved and refined by using the Enraf-Nonius SDP program set to give final discrepancy indices of *R* = 0.060 and *R*<sub>w</sub> = 0.066 with a GOF = 1.11 based on 966 unique data with *F*<sub>o</sub><sup>2</sup> > 2σ(*F*<sub>o</sub><sup>2</sup>). A disordered THF solvent lying on a mirror plane was partially modeled as two overlapping, half-occupancy molecules. The data set was quite limited due to the small size of the crystal. Complete crystallographic details are included in the supplementary material.
- (12) Cf.: (a) Swaminathan, S.; Lessinger, L. *Cryst. Struct. Commun.* **1978**, *7*, 621. (b) Jones, R. O.; Maslen, E. N. *Z. Kristallogr.* **1966**, *123*, 330. (c) Bird, P. H.; Fraser, A. R.; Hall, D. N. *Inorg. Chem.* **1977**, *16*, 1923.

## Articles

Contribution from the Chemical Crystallography Laboratory, University of Oxford, 9 Parks Road, Oxford, OX1 3PD, U.K., Department of Inorganic and Structural Chemistry, Leeds University, Leeds, LS2 9JT, U.K., and Department of Chemistry, University of Oregon, Eugene, Oregon 97403

### Magnetic Structures and Properties of α-CrPO<sub>4</sub> and α-CrAsO<sub>4</sub>

J. Paul Attfield,\*<sup>1a</sup> Peter D. Battle,<sup>1b</sup> Anthony K. Cheetham,<sup>1a</sup> and David C. Johnson<sup>1c</sup>

Received April 5, 1988

The magnetic properties of the isomorphous compounds α-CrPO<sub>4</sub> and α-CrAsO<sub>4</sub> have been investigated by magnetic susceptibility and low-temperature powder neutron diffraction methods. These materials order antiferromagnetically below 9.1 ± 1.0 and 7.7 ± 0.8 K, respectively, and the magnetic structure of α-CrPO<sub>4</sub> at 2 K reveals both ferromagnetic and antiferromagnetic Cr-O-Cr interactions, arising from different linkages of CrO<sub>6</sub> octahedra. The magnetic structure of α-CrAsO<sub>4</sub> at 5 K differs from that of α-CrPO<sub>4</sub> in that the ferromagnetic interactions are frustrated. This is ascribed to the Cr-O-Cr interactions in α-CrAsO<sub>4</sub> being weaker than those in α-CrPO<sub>4</sub>, relative to competing antiferromagnetic interactions through the XO<sub>4</sub> group, as the relevant Cr-O bonds are longer in the former structure.

#### Introduction

Transition-metal oxo salts are of interest because of the wide range of magnetic behavior that they exhibit, enabling the magnetic exchange interactions between the cations to be investigated. As part of this effort, the superexchange interactions between spin-only cations such as Fe(III) and Cr(III) through tetrahedral oxo anions have been studied in a number of MXO<sub>4</sub> compounds, as previously reported.<sup>2-5</sup>

β-CrPO<sub>4</sub><sup>3</sup> and β-CrAsO<sub>4</sub><sup>5</sup> both contain CrO<sub>6</sub> octahedra in infinite, trans edge-sharing chains with XO<sub>4</sub> (X = P, As) tetrahedra linking the chains. Neutron powder diffraction studies have shown that at 5 K the magnetic order along the chains of

(1) (a) University of Oxford. (b) Leeds University. (c) University of Oregon.

(2) Battle, P. D.; Cheetham, A. K.; Gleitzer, C.; Harrison, W. T. A.; Long, G. J.; Longworth, G. J. *Phys. C* **1982**, *15*, L919.  
(3) Attfield, J. P.; Battle, P. D.; Cheetham, A. K. *J. Solid State Chem.* **1985**, *57*, 357.  
(4) Battle, P. D.; Gibb, T. C.; Hu, G.; Munro, D. C.; Attfield, J. P. *J. Solid State Chem.* **1986**, *65*, 343.  
(5) Attfield, J. P.; Cheetham, A. K.; Johnson, D. C.; Torardi, C. C. *Inorg. Chem.* **1987**, *26*, 3379.

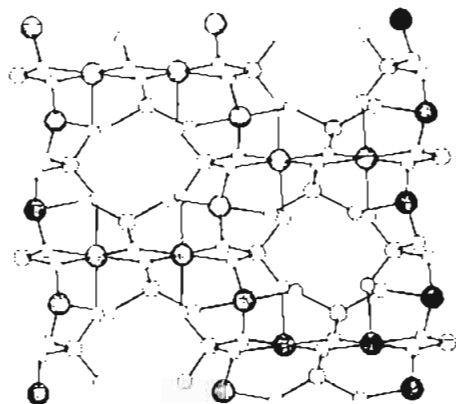


**Figure 1.** Crystal structure of  $\alpha$ -CrPO<sub>4</sub> projected on (100) with  $y$  horizontal and  $z$  vertical: Cr, large shaded circles; P, medium hatched circles; O, small open circles.

octahedra and in the perpendicular plane is antiferromagnetic in both cases but that the two magnetic structures are quite different. In  $\beta$ -CrAsO<sub>4</sub> there is a simple collinear arrangement of moments commensurate with the crystallographic unit cell, while the magnetic structure of  $\beta$ -CrPO<sub>4</sub> consists of a spiral of moments in the plane perpendicular to the chains, with a periodicity of 15.7 Å. However, the differences between these two magnetic structures cannot directly be ascribed to any differences between phosphate and arsenate groups, as the two salts belong to different structure types, with different linkages between chains of octahedra.

Above 1175 °C,  $\beta$ -CrPO<sub>4</sub> transforms to the  $\alpha$  form,<sup>6</sup> which has a crystal structure completely different from that of  $\beta$ -CrPO<sub>4</sub> and other ABO<sub>4</sub> structure types. This structure was solved and refined by using X-ray and neutron powder diffraction data<sup>7,8</sup> and has since been confirmed by a single-crystal study.<sup>9</sup> The structure (Figure 1) consists of an infinite network of linked polyhedra and contains the unusual feature of a CrO<sub>6</sub> octahedron and a PO<sub>4</sub> tetrahedron sharing a common edge. There are 12 Cr<sup>3+</sup> sites per unit cell; the four Cr(1) octahedra are each apically linked to four Cr(2) octahedra, while the eight Cr(2) octahedra form edge-sharing Cr(2), Cr(2') pairs and also share two corners with Cr(1) octahedra. The CrO<sub>6</sub> units build up an infinite, three-dimensional network that might be expected to provide strong Cr—O—Cr magnetic superexchange linkages, and exchange pathways through phosphate groups are also present.

Metastable  $\alpha$ -CrAsO<sub>4</sub> that results from preparations at atmospheric pressure also adopts the  $\alpha$ -CrPO<sub>4</sub> structure,<sup>10</sup> and so we have studied the magnetic properties of these two isomorphs in order to probe both common features due to exchange through this novel network of CrO<sub>6</sub> octahedra and any differences due to the different oxo anions. The only previously reported magnetic investigation of either compound is a magnetic susceptibility study of  $\alpha$ -CrPO<sub>4</sub> between 84.5 and 309.0 K, which revealed a Curie-Weiss curve with  $\theta = -35.1$  K and  $\mu_{\text{eff}} = 3.50 \mu_B$ .<sup>11</sup>

### Experimental Section

Polycrystalline  $\alpha$ -CrAsO<sub>4</sub> was prepared via a solution precursor. Appropriate quantities of Cr(NO<sub>3</sub>)<sub>3</sub>·9H<sub>2</sub>O and 3As<sub>2</sub>O<sub>3</sub>·5H<sub>2</sub>O were dissolved in distilled water, and the solution was heated to dryness in a fume cupboard, giving a brown residue. This was heated at 800 °C for 90 min to produce a fine, green powder. The X-ray diffraction pattern of this material agreed with that reported for  $\alpha$ -CrAsO<sub>4</sub>,<sup>10</sup> but traces of Cr<sub>2</sub>O<sub>3</sub> were also observed and could not be totally eliminated by varying the

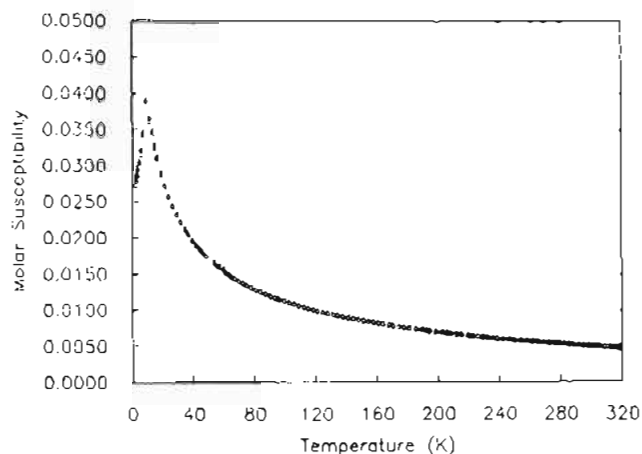


**Figure 2.** Magnetic susceptibility ( $\text{emu mol}^{-1}$ ) of  $\alpha$ -CrPO<sub>4</sub> between 2 and 320 K.

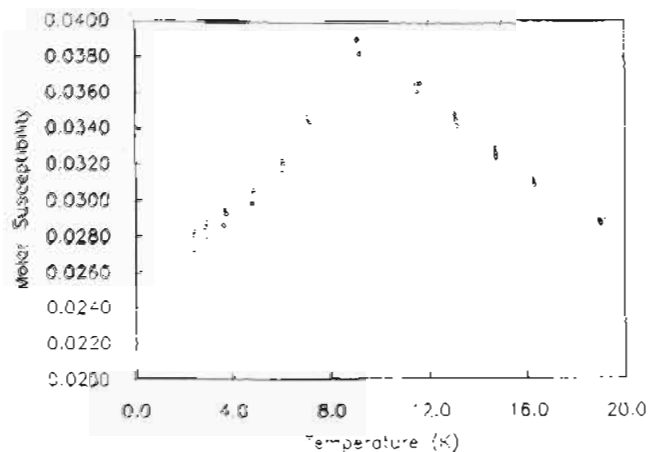


**Figure 3.** Magnetic susceptibility ( $\text{emu mol}^{-1}$ ) of  $\alpha$ -CrPO<sub>4</sub> between 2 and 20 K in applied fields of 15.9 (circles), 18.4 (squares), and 19.5 kG (diamonds).

heating time and temperature. In addition,  $\alpha$ -CrAsO<sub>4</sub> was found to decompose to Cr<sub>2</sub>O<sub>3</sub> and amorphous arsenic oxides on standing at ambient temperatures, so samples were freshly prepared before each experiment. Our synthesis of pure, polycrystalline  $\alpha$ -CrPO<sub>4</sub> has been described elsewhere.<sup>7</sup>

Magnetic susceptibilities were measured on a high-sensitivity Faraday balance at the Experimental Station, E. I. du Pont de Nemours and Co., Wilmington, DE. Data were collected between 2 and 320 K in applied fields between 5.5 and 19.5 kG on a 4.2-mg sample of  $\alpha$ -CrPO<sub>4</sub> and a 15.9-mg sample of  $\alpha$ -CrAsO<sub>4</sub>.

Low-temperature neutron diffraction data were collected on diffractometer D1a at the ILL, Grenoble, France. Initially, 1-h  $6$ – $66^\circ$   $2\theta$  diffraction patterns from  $\sim 10$  g of  $\alpha$ -CrPO<sub>4</sub> in a 16-mm-diameter vanadium can were recorded at a wavelength of 1.95 Å and temperatures of 2.0, 7.5, 12.0, and 15.0 K, in order to monitor the magnetic scattering and any structural changes around  $T_N$ . A 7-h scan from  $6$  to  $156^\circ$   $2\theta$  at 25 K was also performed in order to obtain a good nuclear structure to model the low-temperature data. Unfortunately, a fault in the preamplifier of the lowest angle counter introduced additional intensity into the  $6$ – $12^\circ$  region of these scans, which contains the most intense magnetic diffraction peak, and these data could not be used for magnetic structure determination. The diffraction pattern of  $\alpha$ -CrPO<sub>4</sub> was re-collected at 2 K by performing two 2.5-h scans from  $6$  to  $67^\circ$  and from  $66$  to  $127^\circ$   $2\theta$  on the D1a diffractometer and combining the data. This procedure was used in order to obtain even counting statistics across the whole profile in view of the intense magnetic peak at  $8^\circ$   $2\theta$ . The powder diffraction profile of  $\alpha$ -CrAsO<sub>4</sub> at 5 K was recorded between  $6$  and  $150^\circ$   $2\theta$  in 16 h by the usual continuous-scan method.

### Results

**Magnetic Susceptibility Measurements.** The molar susceptibility data for  $\alpha$ -CrPO<sub>4</sub> displayed in Figures 2 and 3 show a sharp antiferromagnetic transition at  $T_N = 9.1 \pm 1.0$  K. No field variation of  $T_N$  is apparent, indicating that there is no ordered ferromagnetic component. (The apparent field dependence of the

- (6) Shafer, M. W.; Roy, R. *J. Am. Chem. Soc.* **1956**, *78*, 1087.
- (7) Attfield, J. P.; Sleight, A. W.; Cheetham, A. K. *Nature (London)* **1986**, *322*, 620.
- (8) Attfield, J. P.; Cheetham, A. K.; Cox, D. E.; Sleight, A. W. *J. Appl. Crystallogr.* **1988**, *21*, 452.
- (9) Glaum, R.; Gruhn, R.; Moller, M. *Z. Anorg. Allg. Chem.* **1986**, *543*, 111.
- (10) Ronis, M. M. *C. R. Seances Acad. Sci., Ser. C* **1970**, *271C*, 64.
- (11) Lukaszewski, G. M.; Redfern, J. P. *J. Chem. Soc.* **1963**, 3790.

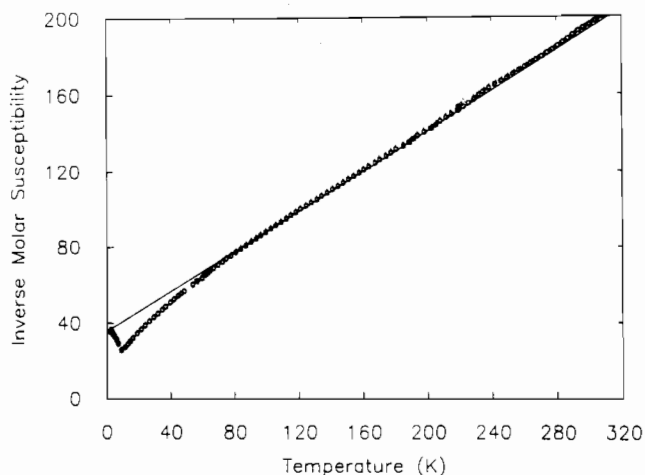


**Figure 4.** Inverse magnetic susceptibility ( $\text{emu}^{-1} \text{mol}$ ) of  $\alpha$ -CrPO<sub>4</sub> between 2 and 320 K, with the Curie-Weiss fit shown.

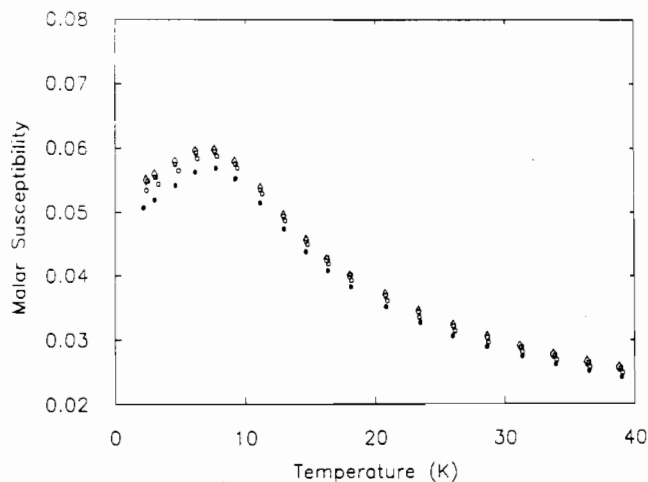


**Figure 5.** Magnetic susceptibility ( $\text{emu mol}^{-1}$ ) of  $\alpha$ -CrAsO<sub>4</sub> between 2 and 40 K in applied fields of 5.3 (filled circles), 15.9 (open circles), 18.4 (squares), and 19.5 kG (diamonds).

low-temperature susceptibility is not due to ferromagnetism as the susceptibility *increases* with increasing field. It is perhaps due to field calibration errors or small lateral displacements of the sample in high fields.) The inverse susceptibility of  $\alpha$ -CrPO<sub>4</sub> in Figure 4 follows the Curie-Weiss law at high temperatures with  $\Theta = -67.7$  K and  $\mu_{\text{eff}} = 3.89 \mu_{\text{B}}$ . The latter is close to the expected value for spin-only  $S = 3/2$  ions ( $\mu_{\text{SO}} = 3.87 \mu_{\text{B}}$ ), unlike the anomalous value of  $3.50 \mu_{\text{B}}$  reported previously,<sup>11</sup> suggesting that an impure sample was used in that work. As the Curie-Weiss behavior breaks down with decreasing temperature, there is a pronounced deviation of the inverse susceptibility below the Curie-Weiss limit until the ordering temperature is reached.

The magnetic susceptibility curve of  $\alpha$ -CrAsO<sub>4</sub> is similar to that of  $\alpha$ -CrPO<sub>4</sub>, although the antiferromagnetic transition at  $T_{\text{N}} = 7.7 \pm 0.8$  K (Figure 5) is broader than that in  $\alpha$ -CrPO<sub>4</sub>. A Curie-Weiss fit to the inverse susceptibility data at high temperatures gives  $\Theta = -33.7$  K and  $\mu_{\text{eff}} = 3.80 \mu_{\text{B}}$ . A slight deviation of the inverse paramagnetic susceptibility below the Curie-Weiss limit occurs close to  $T_{\text{N}}$ , as in  $\alpha$ -CrPO<sub>4</sub>.

**Powder Neutron Diffraction.** Nuclear and magnetic structure refinements were performed by the Rietveld profile technique.<sup>12</sup> The structure of  $\alpha$ -CrPO<sub>4</sub> refined by using the 25 K powder neutron diffraction data has been described elsewhere<sup>7</sup> and shows that no structural distortion takes place on cooling from room temperature to 25 K. These coordinates were used to fit the nuclear part of the 2.0–15.0 K scans of  $\alpha$ -CrPO<sub>4</sub> in space group *Imma* (No 74). The cell constants were refined by using the

**Table I.** Cell Parameters and Volumes (with Esd's in Parentheses) of  $\alpha$ -CrPO<sub>4</sub> at 2.0, 7.5, 12.0, and 15.0 K Refined by Using  $6-66^\circ 2\theta$  Neutron Profiles

	2.0 K	7.5 K	12.0 K	15.0 K
cell params, Å				
<i>a</i>	10.3748 (6)	10.3740 (6)	10.3746 (6)	10.3742 (6)
<i>b</i>	12.8456 (9)	12.8467 (9)	12.8463 (9)	12.8472 (9)
<i>c</i>	6.2790 (4)	6.2785 (4)	6.2778 (4)	6.2784 (4)
cell vol, Å <sup>3</sup>	836.80 (6)	836.74 (6)	836.68 (6)	836.79 (6)

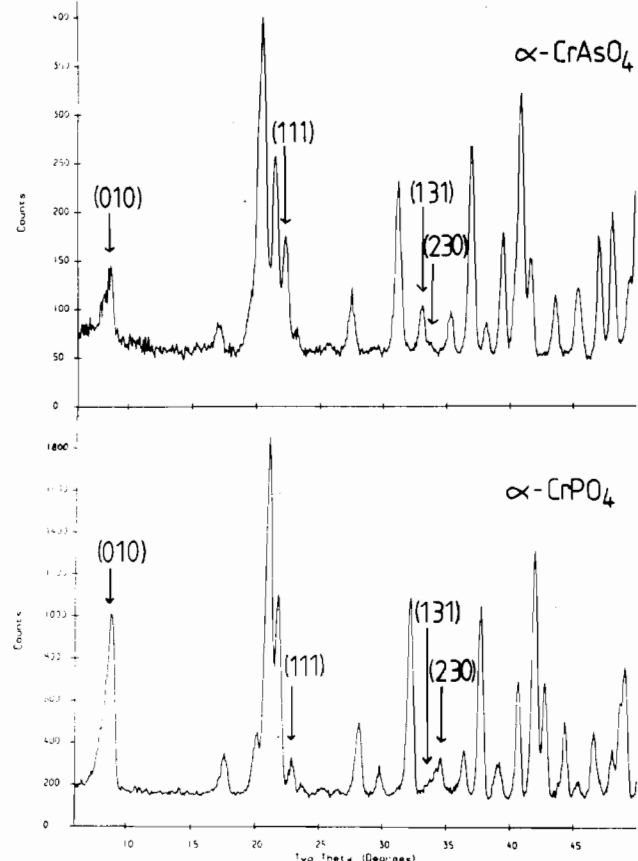


**Figure 6.** Low-angle regions of the neutron diffraction patterns of  $\alpha$ -CrAsO<sub>4</sub> at 5 K and  $\alpha$ -CrPO<sub>4</sub> at 2 K, with magnetic peaks labeled ( $\lambda = 1.95$  Å).

2.0–15.0 K data with the zero-point error in counter position fixed at the value obtained from the 25 K refinement, and the results are presented in Table I. Magnetic diffraction was observed in the 2.0 and 7.5 K patterns.

The low-angle regions of the  $6-127^\circ$  pattern of  $\alpha$ -CrPO<sub>4</sub> at 2.0 K and the diffraction profile of  $\alpha$ -CrAsO<sub>4</sub> at 5.0 K are shown in Figure 6 with magnetic reflections labeled. All of the observed magnetic peaks in both patterns could be indexed on the orthorhombic atomic unit cell with odd  $h + k + l$  and  $k$  values. The former reflection condition implies that the moments on cations related by a body-centering translation are antiparallel ( $P_1$  magnetic symmetry), and consideration of the terms in the magnetic structure factor shows that the second condition is consistent with moments on sites related by the mirror plane at  $(x, 1/4, z)$  being paired. These two magnetic symmetry operations are sufficient to define the relative orientations of the four Cr(1) moments but give two possible modes for the arrangement of the eight Cr(2) moments, as shown in Table II. The four Cr(1) spins contribute to both (eoe) and (ooo) magnetic reflections (o and e represent odd and even integers, respectively), whereas the eight Cr(2) moments give rise only to (eoe) peaks if aligned according to mode A and only to (ooo) reflections from mode B. Comparison of the magnetic peak intensities in Figure 6 shows that the (eoe) reflections are more intense than the (ooo) peaks in the  $\alpha$ -CrPO<sub>4</sub> profile, but the (ooo) peaks predominate in the pattern of  $\alpha$ -CrAsO<sub>4</sub>, suggesting that the Cr(2) moments are aligned according

(12) Rietveld, H. M. *J. Appl. Crystallogr.* **1969**, *2*, 65.

**Table II.** Allowed Modes for the Four Cr(1) and Eight Cr(2) Spins in the Unit Cells of  $\alpha$ -CrPO<sub>4</sub> and  $\alpha$ -CrAsO<sub>4</sub>, Consistent with the Observed Magnetic Reflections, and Allowed Reflections Due to Each Spin Arrangement, in Which o Represents an Odd Value of  $h$ ,  $k$ , or  $l$  and e Stands for an Even or Zero Value

Cr(1) spins					
position	spin direction	position	spin direction		
$(\frac{1}{2}, \frac{1}{2}, 0)$	+	$(0, \frac{1}{2}, \frac{1}{2})$	+	magnetic reflns (eoe) and (ooo)	
$(\frac{1}{2}, 0, 0)$	-				
$(0, 0, \frac{1}{2})$	-				
Cr(2) spins					
position	spin direction		position	spin direction	
	mode A	mode B		mode A	mode B
$(\frac{1}{4}, y, \frac{1}{4})$	+	+	$(\frac{3}{4}, -y, \frac{3}{4})$	+	+
$(\frac{1}{4}, \frac{1}{2}-y, \frac{1}{4})$	-	-	$(\frac{1}{4}, \frac{1}{2}+y, \frac{3}{4})$	-	+
$(\frac{3}{4}, y, \frac{1}{4})$	+	-	$(\frac{1}{4}, -y, \frac{3}{4})$	+	-
$(\frac{3}{4}, \frac{1}{2}-y, \frac{1}{4})$	-	+	magnetic reflns	(eoe)	(ooo)
$(\frac{3}{4}, \frac{1}{2}+y, \frac{3}{4})$	-	-			

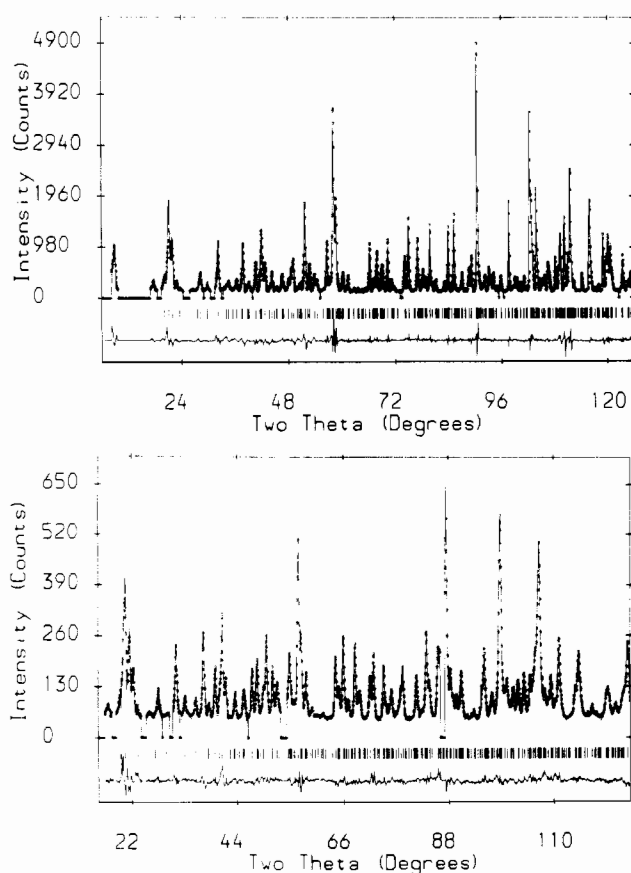


**Figure 7.** Observed (points), calculated (full line), and difference neutron diffraction profiles for (a, top)  $\alpha$ -CrPO<sub>4</sub> at 2 K and (b, bottom)  $\alpha$ -CrAsO<sub>4</sub> at 5 K.

to mode A in the former compound and mode B in the latter.

The nuclear part of the  $\alpha$ -CrPO<sub>4</sub> diffraction pattern was fitted by refining the 25 K structural model and then held constant while the magnetic scattering from trial spin arrangements was calculated. Only models with Cr(2) spins aligned in mode A gave a reasonable fit to the data; the best consisted of adjacent Cr(1) and Cr(2) moments lying parallel in the  $yz$  plane. Attempts to refine this model with the asymmetric, low angle (010) peak excluded from the calculation did not give sensible results due to the weakness of the other magnetic reflections, and even when this reflection was included, it was not possible to refine the magnitudes and directions of the Cr(1) and Cr(2) moments due to errors arising from the peak asymmetry. To overcome this, the magnitudes of the moments were fixed at a typical value of

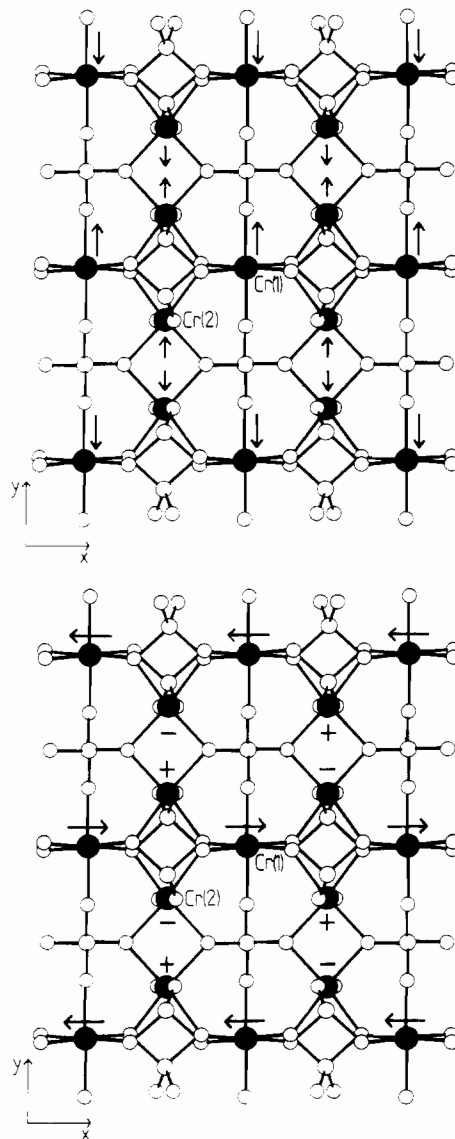


**Figure 8.** Atomic and magnetic structures of (a, top)  $\alpha$ -CrPO<sub>4</sub> and (b, bottom)  $\alpha$ -CrAsO<sub>4</sub> projected on (001) with the magnetic ions shown as shaded circles.

$2.4 \mu_B$ , based on other refinements of CrXO<sub>4</sub> magnetic structures,<sup>5,13</sup> and their directions were varied in the  $yz$  plane. When adjacent Cr(1) and Cr(2) spins were held parallel, the refinement gave  $R_{WP} = 12.7\%$  and  $R_{MAG} = 30.1\%$ <sup>14</sup> with moments tilted 53 (1) $^\circ$  from  $c$ . Allowing these two spins to vary independently in the  $yz$  plane improved the magnetic fit; the final refinement of the nuclear and magnetic structures converged to  $R_{WP} = 12.6\%$ ,  $R_{MAG} = 26.2\%$ , and  $\chi^2 = 3.49$  with the Cr(1) and Cr(2) moments tilted by 70 (1) and 36 (1) $^\circ$ , respectively, from the  $z$  axis.

The crystal structure of  $\alpha$ -CrAsO<sub>4</sub> at 5 K was refined in  $Imma$  by using the  $\alpha$ -CrPO<sub>4</sub> structure as a starting model. Magnetic reflections were not included, and profile data above 126 $^\circ$   $2\theta$  were also excluded from the refinement due to excessive peak broadening. The resulting difference profile revealed small diffraction peaks from Cr<sub>2</sub>O<sub>3</sub> at 53 and 87 $^\circ$   $2\theta$ , which were excluded from all future refinements. The magnetic reflections were then included in the refinement, and a model with the Cr(1) and Cr(2) spins parallel to the  $x$  and  $z$  axes, respectively, gave a good fit when the Cr(2) moments were arranged according to mode B. In this case it proved possible to refine the magnetic structure without including the asymmetric (010) peak by constraining the Cr(1) and Cr(2) moments to have equal magnitudes. The final refinement of all the atomic parameters gave  $R_{WP} = 9.9\%$ ,  $R_{MAG}$

(13) Attfield, J. P. D. Phil. Thesis, University of Oxford, 1987.

(14) The  $R$  factors are defined in ref 12.

**Table III.** Results of the Refinement of the Crystal and Magnetic Structures of  $\alpha$ -CrPO<sub>4</sub> at 2.0 K (P) and  $\alpha$ -CrAsO<sub>4</sub> at 5.0 K (As) Using Powder Neutron Data (Esd's in Parentheses)

		P	As					
no. of profile points		2140	2098					
no. of refined params		23	22					
$\chi^2$		3.49	2.32					
overall $B_{iso}$ , Å <sup>2</sup>		0.02 (3)	0.23 (2)					
cell constants, Å								
		a	b	c				
P		10.3797 (1)	12.8452 (2)	6.2797 (1)				
As		10.5466 (1)	13.2424 (1)	6.4612 (1)				
R factors, %								
		$R_{WP}$	$R_P$	$R_{NUC}$	$R_{MAG}$	$R_{EX}$		
P		12.6	11.5	4.5	26.2	6.7		
As		9.9	9.6	5.3	16.1	6.5		
		fractional coordinates in <i>Imma</i> (No. 74)			magnetic components, $\mu_B^a$			
atom	symmetry position	x	y	z	$\mu_x$	$\mu_y$	$\mu_z$	
Cr(1)	4b	P	1/2	1/2	0	0	2.26 (2)	0.80 (6)
		As				2.44 (4)	0	0
Cr(2)	8g	P	1/4	0.3648 (4)	1/4	0	1.41 (6)	1.94 (5)
		As		0.3607 (5)		0	0	-2.44 (4)
P(1)	4e		1/2	1/4	0.0838 (8)			
As(1)					0.0642 (7)			
P(2)	8g		1/4	0.5740 (3)	1/4			
As(2)					0.5748 (2)			
O(1)	8i	P	0.3780 (3)	1/4	0.2265 (5)			
		As	0.3701 (4)		0.2195 (6)			
O(2)	16j	P	0.3607 (2)	0.4900 (2)	0.2138 (4)			
		As	0.3646 (3)	0.4817 (2)	0.2077 (4)			
O(3)	16j	P	0.2235 (2)	0.6367 (2)	0.0554 (3)			
		As	0.2138 (2)	0.6407 (2)	0.0451 (3)			
O(4)	8h	P	1/2	0.3488 (3)	-0.0444 (5)			
		As		0.3551 (3)	-0.0761 (4)			

<sup>a</sup>The magnetic moments in  $\alpha$ -CrPO<sub>4</sub> were constrained to lie in the *yz* plane and to have a total magnitude of 2.4  $\mu_B$ .

**Table IV.** Bond Distances (Å) from the Refinements of  $\alpha$ -CrXO<sub>4</sub> Structures (X = P, As) with Esd's in Parentheses

	X = P	X = As
Cr(1)-O(2) (×4)	1.977 (2)	1.982 (3)
Cr(1)-O(4) (×2)	1.960 (3)	1.980 (3)
Cr(2)-O(1) (×2)	1.991 (9)	1.95 (1)
Cr(2)-O(2) (×2)	1.989 (8)	2.03 (1)
Cr(2)-O(3) (×2)	1.936 (8)	1.944 (9)
X(1)-O(1) (×2)	1.552 (7)	1.702 (8)
X(1)-O(4) (×2)	1.507 (8)	1.661 (7)
X(2)-O(2) (×2)	1.591 (5)	1.751 (6)
X(2)-O(3) (×2)	1.493 (5)	1.634 (5)

= 16.1%,  $\chi^2 = 2.32$ , and a magnetic moment of 2.44 (4)  $\mu_B$ .

The atomic parameters and bond distances and angles from both refinements are presented in Tables III and IV, and observed, calculated, and difference plots are shown in Figure 7. Projections of the magnetic structures on (001) are displayed in Figure 8.

### Discussion

$\alpha$ -CrPO<sub>4</sub> and  $\alpha$ -CrAsO<sub>4</sub> display very similar variations of magnetic susceptibility with temperature, and both order antiferromagnetically below 10 K. The width of the transition in the  $\alpha$ -CrAsO<sub>4</sub> data may reflect the poor crystallinity of this phase. At high temperatures these materials behave as Curie-Weiss paramagnets with spin-only moments and negative values of  $\Theta$ , reflecting dominant antiferromagnetic interactions between the spins, but as the temperature is lowered toward  $T_N$ , the inverse susceptibility deviates below the Curie-Weiss limit, which is unusual as this indicates short-range ferromagnetic order. The magnitudes of  $\Theta$  and  $T_N$  for  $\alpha$ -CrAsO<sub>4</sub> are smaller than those for  $\alpha$ -CrPO<sub>4</sub> due to the increased separation of the Cr<sup>3+</sup> cations by the larger arsenate group, which weakens the superexchange interactions.

Fits to the neutron scans of  $\alpha$ -CrPO<sub>4</sub> between 2.0 and 15.0 K do not reveal any distortions of the cell on magnetic ordering, nor are there any large differences between the atomic positions at

2, 25,<sup>7</sup> and 300 K.<sup>8</sup> This suggests that the strain imposed by this arrangement of polyhedra cannot be relieved by a simple structural distortion.

The profile refinement of the crystal and magnetic structures of  $\alpha$ -CrPO<sub>4</sub> at 2 K gives a relatively high value of  $\chi^2$ , due in part to small errors in the positions of individual counters arising from the scan procedure used; this gives rise to the features in the difference profile (Figure 7a) around 58, 90, and 110° 2 $\theta$ . Discrepancies are also observed due to peak symmetry at low angles, as the empirical correction due to Rietveld,<sup>12</sup> which was applied to reflections below 24°, does not completely model this effect. The gross asymmetry of the dominant magnetic peak at 8° 2 $\theta$  may account for the relatively high value of  $R_{MAG}$ , in view of which the difference between the fits with canted and parallel Cr(1) and Cr(2) spins may not be significant. A statistically better fit is obtained for  $\alpha$ -CrAsO<sub>4</sub> at 5 K, reflecting the continuous-scan method of data collection and the fact that it proved possible to refine the magnetic structure with the (001) peak excluded.

The geometric effects of replacing phosphate by arsenate in the  $\alpha$ -CrPO<sub>4</sub> structure type can be seen by comparing the distances and angles in Table IV. Although the arsenate group is larger and less rigid than the phosphate anion, and so should be more able to accommodate the strain imposed by this structure, there seems to be little change in the Cr<sup>3+</sup> cation geometry. The variation in As-O bond distances from 1.63 to 1.75 Å is comparable to that in  $\beta$ -CrAsO<sub>4</sub>.<sup>5</sup>

$\alpha$ -CrPO<sub>4</sub> and  $\alpha$ -CrAsO<sub>4</sub> order as four sublattice antiferromagnets at low temperatures, and there is no evidence for an ordered ferromagnetic component in either case. In both magnetic structures, spins on neighboring, edge-sharing octahedral Cr(2) and Cr(2') sites at (1/4, *y*, 1/4) and (1/4, 1/2 - *y*, 1/4) are antiparallel due to antiferromagnetic interactions arising from the overlap of half-filled cation *t*<sub>2g</sub> orbitals and filled O 2*p* <sub>$\pi$</sub>  orbitals and possibly a direct Cr-Cr overlap as well ( $d(\text{Cr}(2)\text{-Cr}(2')) = 2.95$  Å in  $\alpha$ -CrPO<sub>4</sub>, 2.93 Å in  $\alpha$ -CrAsO<sub>4</sub>). Magnetic anisotropy, resulting in part from favorable dipole-dipole interactions, causes the spins

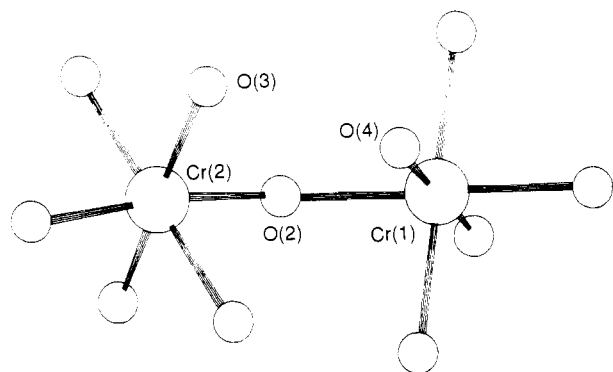
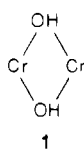


**Figure 9.** Geometry of the apically linked Cr(1) and Cr(2) octahedra in the  $\alpha$ -CrPO<sub>4</sub> structure. Different degrees of twisting of the octahedra out of the Cr(1)-O(2)-Cr(2) plane are illustrated by the Cr(2)-O(2)-Cr(1)-O(4) and O(3)-Cr(2)-O(2)-Cr(1) dihedral angles, which are 16 and 42°.

to lie along  $z$  in  $\alpha$ -CrAsO<sub>4</sub> and to lie 36 (1)° from  $z$  in the  $yz$  plane in  $\alpha$ -CrPO<sub>4</sub>. However, the two magnetic structures differ in the relative alignment of the four Cr(2), Cr(2') spin pairs in the unit cell and the orientation of the Cr(1) moments.

In  $\alpha$ -CrPO<sub>4</sub> the Cr(2) spins order according to mode A in Table II, and each Cr(1) spin is connected to four parallel Cr(2) spins by equivalent Cr(1)-O-Cr(2) linkages in which the bridging angle is 123.5°. The Cr(1) and neighboring Cr(2) moments are essentially parallel, indicating a ferromagnetic Cr(1)-O-Cr(2) exchange interaction. This is unusual, as Cr-O-Cr interactions have been found to result in antiferromagnetic exchange with a wide variety of bridging angles<sup>15</sup> but can be rationalized from the fact that the Cr(1) and Cr(2) octahedra are twisted out of the Cr(1)-O-Cr(2) plane by 16 and 42° respectively, as shown in Figure 9. As the  $t_{2g}$  orbitals lie between each pair of oxygen ligands, good mutual  $\pi$ -overlap of  $t_{2g}$  orbitals from each cation with a bridging O  $2p_{\pi}$  orbital, which would favor antiferromagnetic exchange, is not possible. A direct Cr-Cr interaction is also prevented by the disposition of the  $t_{2g}$  orbitals and the Cr(1)-Cr(2) distance of 3.49 Å. Instead, potential exchange between the spins predominates, resulting in a ferromagnetic ground state. Such ferromagnetic Cr<sup>3+</sup>-O-Cr<sup>3+</sup> couplings are rare; another example has been reported in the trirutile WCr<sub>2</sub>O<sub>6</sub>,<sup>15</sup> in which there is a similar twisted CrO<sub>5</sub>-O-CrO<sub>5</sub> geometry and a bridging angle of ~130°. Ferromagnetic interactions through the bridge **1** have



also been observed in a few binuclear complexes<sup>17,18</sup> when the tilting angle of the O-H bond out of the Cr-O-Cr plane is large, as the O  $2p_z$  orbital participates in  $\sigma$ (O-H) bonding that weakens the antiferromagnetic Cr-O-Cr  $\pi$ -superexchange interaction.

The Cr(2), Cr(2') spin pairs in  $\alpha$ -CrAsO<sub>4</sub> follow the B mode of alignment in Table II, and each Cr(1) spin is equally connected to two "up" and two "down" Cr(2) spins, so the symmetric Heisenberg exchange interactions ( $-2J_1S_1 \cdot S_2$ ) of the Cr(1) spin with these four neighbors sum to zero whatever the spin direction. Under such circumstances, weaker effects such as the antisymmetric Dzyaloshinsky-Moriya exchange interaction ( $D_{12}(S_1 \times$

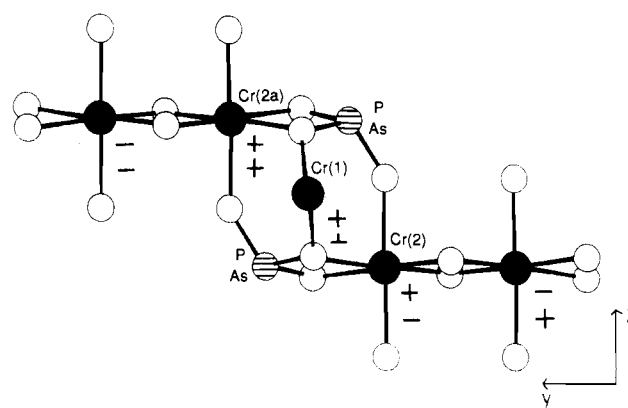


**Figure 10.** Linkages between the Cr(2) spin at  $(\frac{1}{4}, y, \frac{1}{4})$  and Cr(2a) at  $(\frac{1}{4}, -y, \frac{3}{4})$  in the  $\alpha$ -CrPO<sub>4</sub> structure type: Cr, shaded circles; P/As, striped circles; O, open circles. Relative spin directions in  $\alpha$ -CrPO<sub>4</sub> are shown as + and -, neglecting the canting between neighboring Cr(1) and Cr(2) spins, and those in  $\alpha$ -CrAsO<sub>4</sub> are given below by using  $\perp$  to indicate that the Cr(1) spins are perpendicular to the Cr(2) moments.

$S_2$ ), where  $D_{12}$  is a constant vector)<sup>19-21</sup> may determine the Cr(1) spin direction. In this structure there are no symmetry restrictions on  $D_{12}$ , as Cr(1) and Cr(2) are crystallographically independent. The Dzyaloshinsky-Moriya interaction favors a perpendicular spin arrangement and is consistent with the observed magnetic structure in which the Cr(1) and Cr(2) spins are parallel to the orthorhombic  $x$  and  $z$  axes, respectively. The strength of the Dzyaloshinsky-Moriya interaction depends upon the anisotropy of the system, which is small in octahedrally coordinated Cr<sup>3+</sup>, so these effects only become significant when the Heisenberg interactions are frustrated, as is the case in  $\alpha$ -CrAsO<sub>4</sub>.

The cause of the differences between the magnetic structures of  $\alpha$ -CrPO<sub>4</sub> and  $\alpha$ -CrAsO<sub>4</sub> must lie in the differences in geometry of the exchange pathways in the two materials. Figure 10 shows the pertinent linkages between Cr(2) spins at  $(\frac{1}{4}, y, \frac{1}{4})$  and  $(\frac{1}{4}, -y, \frac{3}{4})$ . The Cr(2)-O-Cr(1)-O-Cr(2) pathway favors parallel alignment of the Cr(2) spins through two ferromagnetic Cr(2)-O-Cr(1) interactions, while the two Cr(2)-O-X-(O)<sub>2</sub>-Cr(2) superexchange pathways through the nonmagnetic X atom give rise to antiferromagnetic exchange between the Cr(2) spins. The major differences between the magnetic structures of  $\alpha$ -CrPO<sub>4</sub> and  $\alpha$ -CrAsO<sub>4</sub> can all be rationalized on the basis of the two different outcomes of the competition between these superexchange interactions. If the exchange through Cr(1) is stronger than the antiferromagnetic couplings through the phosphate groups in  $\alpha$ -CrPO<sub>4</sub>, then a parallel alignment of the Cr(1) and two Cr(2) spins results and there is no magnetic frustration. However, if in  $\alpha$ -CrAsO<sub>4</sub> antiferromagnetic exchange through the two arsenate groups is stronger than the Cr(2)-O-Cr(1)-O-Cr(2) interaction, then the Cr(2) spins at  $(\frac{1}{4}, y, \frac{1}{4})$  and  $(\frac{3}{4}, -y, \frac{1}{4})$  in Figure 10 adopt an antiparallel orientation and the intermediate Cr(1) spin lies perpendicular to both due to antisymmetric couplings, as the ferromagnetic Heisenberg exchange interactions are totally frustrated. The Dzyaloshinsky-Moriya interactions result in an antiparallel alignment of the next-nearest-neighbor Cr(2) spins at  $(\frac{1}{4}, y, \frac{1}{4})$  and  $(\frac{3}{4}, y, \frac{1}{4})$ .

The reasons for these two different spin arrangements lie mainly in the lengths of the exchange pathways, as the strength of superexchange interactions is known to be strongly dependent upon distance.<sup>22</sup> The through-bond lengths of the Cr(2)-O-Cr(1)-O-Cr(2) pathways are 7.93 (1) and 8.02 (1) Å, and the Cr(2)-O-X-O-Cr(2) distances are 7.01 (1) and 7.36 (2) Å, in  $\alpha$ -CrPO<sub>4</sub> and  $\alpha$ -CrAsO<sub>4</sub>, respectively. The difference in the lengths of the latter pathway of 0.35 (2) Å corresponds to the difference between the sizes of tetrahedral P(V) and As(V) ( $2r(\text{As})$

(15) Hodgson, D. J. In *Magneto-Structural Correlations in Exchange Coupled Systems*; NATO ASI Series Vol. C140; Willett, R. D., Gatteschi, D., Kahn, O., Eds.; D. Reidel: Dordrecht, The Netherlands, 1985; see also references therein.

(16) Drillon, M.; Padel, L.; Bernier, J. C. *J. Chem. Soc., Faraday Trans. 2* **1980**, *76*, 1224.

(17) Scaringe, R. P.; Hatfield, W. E.; Hodgson, D. J. *Inorg. Chem.* **1977**, *16*, 1600.

(18) Reber, C.; Gudel, H. U.; Spiccia, L.; Marty, W. *Inorg. Chem.* **1987**, *26*, 3186.

(19) Dzyaloshinsky, I. *J. Phys. Chem. Solids* **1958**, *4*, 241.

(20) Moriya, T. *Phys. Rev.* **1960**, *117*, 635.

(21) Moriya, T. *Phys. Rev.* **1960**, *120*, 91.

(22) de Jongh, L. J.; Block, R. *Physica B+C* **1975**, *79B+C*, 568.

$-2r(\text{P}) = 0.33 \text{ \AA}$ ),<sup>23</sup> and so this does not necessarily weaken the superexchange interaction. However, the small difference in the distances of the Cr(2)-O-Cr(1)-O-Cr(2) pathway will result in this interaction being weaker in  $\alpha\text{-CrAsO}_4$  than in  $\alpha\text{-CrPO}_4$ . Hence, the differences in the magnetic structures of  $\alpha\text{-CrPO}_4$  and  $\alpha\text{-CrAsO}_4$  can be attributed to this indirect effect of the Cr-O distances being slightly longer in the latter material, rather than superexchange through the arsenate group being any stronger than that through phosphate.

The presence of antiferromagnetic and weaker ferromagnetic Cr-O-Cr interactions accounts for the magnetic susceptibility variations of these materials. The frustrations due to the competing superexchange pathways result in large  $|\theta/T_N|$  ratios although the magnetic ordering has three-dimensional characteristics. Antiferromagnetic Curie-Weiss behavior is observed when  $T \gg T_N$ , but as  $T \rightarrow T_N$ , there is a rise in the susceptibility due to short-range ferromagnetic order arising from the Cr(1)-O-

Cr(2) interactions. Below  $T_N$  there is a rapid decrease in the short-range ferromagnetic order, and the system tends to anti-ferromagnetism as  $T \rightarrow 0$ . Thus, no field dependence develops below  $T_N$ , in contrast to  $\beta\text{-CrAsO}_4$ ,<sup>5</sup> in which an ordered weak ferromagnetic component was observed by susceptibility measurements over the same field range. This difference may be explained by the magnetic symmetries of the ordered states; both  $\alpha\text{-CrPO}_4$  and  $\alpha\text{-CrAsO}_4$  belong to  $P_1$  magnetic groups that cannot allow a ferromagnetic component, whereas  $\beta\text{-CrAsO}_4$  belongs to a primitive magnetic group that also permits a ferromagnetic component.<sup>5</sup>

**Acknowledgment.** We are grateful to R. S. McLean for measuring the magnetic susceptibilities and to the SERC for providing a studentship for J.P.A. and neutron facilities. J.P.A. thanks Christ Church, Oxford, for a Junior Research Fellowship.

**Registry No.**  $\alpha\text{-CrPO}_4$ , 7789-04-0;  $\alpha\text{-CrAsO}_4$ , 15070-22-1.

**Supplementary Material Available:** A table of bond angles in  $\alpha\text{-CrPO}_4$  at 2 K and  $\alpha\text{-CrAsO}_4$  at 5 K (1 page). Ordering information is given on any current masthead page.

(23) Shannon, R. D. *Acta Crystallogr.* 1976, A32, 751.

Contribution from the Anorganisch-Chemisches Institut der Universität Münster, Wilhelm-Klemm-Strasse 8, D-4400 Münster, FRG, Department of Chemistry and Materials Science Center, Cornell University, Ithaca, New York 14853-1301, and School of Chemistry, University of Hyderabad, P.O. Central University, Hyderabad 500 134, India

## The Richness of Structures Available to $\text{CpMS}_4\text{MCp}$ Complexes

Wolfgang Tremel,<sup>†,‡</sup> Roald Hoffmann,<sup>\*,§</sup> and Eluvathingal D. Jemmis<sup>||</sup>

Received April 19, 1988

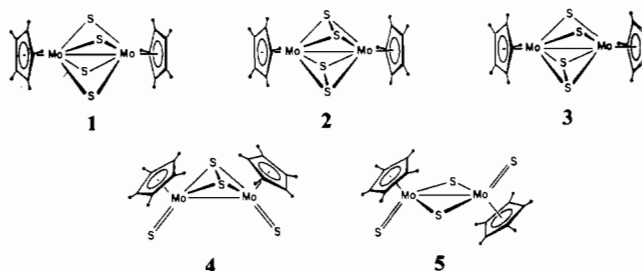
Compounds with the general formula  $\text{CpMS}_4\text{MCp}$  display a remarkable variety in structure. By a detailed theoretical analysis of this class of complexes and related compounds such as  $\text{NbX}_2\text{Y}_6$  ( $X = \text{Se, Te; Y = Br, I}$ ) or  $\text{CpV}(\text{S}_2)_2\text{S}_2\text{VCp}$ , we are able to explain how the central  $\text{S}_4$  unit traverses in many compounds a range in S-S bonding from a ring to isolated sulfide bridges. The isomer  $\text{CpMo}(\text{S}_2)_2\text{MoCp}$  can undergo a symmetry-allowed transformation to form  $\text{CpMo}(\text{S})\text{S}_2(\text{S})\text{MoCp}$ . The bonding in the molecular compounds is compared to that in their solid-state analogues  $\text{NbX}_2\text{Y}_6$ . As in acetylene complexes,  $\text{S}_2$  groups can enter the compounds under study in a parallel and a perpendicular orientation. The latter one is energetically preferred. The rearrangement of parallel- and perpendicular-oriented  $\text{S}_2$  groups is symmetry forbidden.

### Introduction

The strong affinity of chalcogenides for elements of the transition series is the basis for a variety of metal sulfur compounds. Metal sulfides are the most important class of naturally occurring metal ores.<sup>1</sup> Parallel to this, the chalcogenides display a broad range of capabilities as construction units in the design of stable transition-metal clusters.<sup>2</sup> Typical goals in this heavily investigated area of inorganic chemistry include the synthesis of models for important biological<sup>3</sup> and industrial<sup>4</sup> catalysts and the preparation of materials for energy storage and conversion.<sup>5</sup> A particular incentive is the prospect that discrete metal chalcogenide clusters may prove to be functional analogues of the active sites of nitrogenase<sup>6</sup> and hydrodesulfurization catalysts.<sup>7</sup>

Numerous complexes have been synthesized and structurally characterized, pointing to the extremely versatile ligand behavior of elemental sulfur. It can enter transition-metal compounds in many guises, as sulfide,<sup>2</sup> disulfide,<sup>8</sup> or polysulfide.<sup>9</sup> Each of these sulfur ligands can be linked to several metal atoms. Unsubstituted sulfur, for example, has been reported (besides its occurrence in a terminal position) in doubly,<sup>2</sup> triply,<sup>2,10</sup> quadruply,<sup>10a,11</sup> 5-fold,<sup>12</sup> and 6-fold<sup>13</sup> bridging geometries.

Given this richness in coordination, it is not surprising that several isomers of the title compound are known. Some of them are shown in 1-5.<sup>14</sup> In structures 1-3 two CpMo fragments are bridged by four S atoms, two of which have transformed into



terminal ligands in 4<sup>14b</sup> and 5.<sup>14d</sup> Still more isomers can be thought of. Among those that exist 3<sup>14c</sup> and 5<sup>14d</sup> have been structurally

- (1) Vaughn, D. J.; Craig, J. R. *Mineral Chemistry of Metal Sulfides*; Cambridge University Press: Cambridge, U.K., 1978.
- (2) Vahrenkamp, H. *Angew. Chem.* 1975, 87, 363; *Angew. Chem., Int. Ed. Engl.* 1975, 14, 322.
- (3) (a) Coughlin, M. P., Ed. *Molybdenum and Molybdenum Containing Enzymes*; Pergamon Press: Oxford, U.K., 1980. (b) Lovenberg, W., Ed. *Iron Sulfur Proteins*; Academic Press: New York, 1976. (c) Spiro, T. G., Ed. *Iron Sulfur Proteins*; Academic Press: New York, 1982.
- (4) (a) Weisser, O.; Landa, S. *Sulfide Catalysts, Their Properties and Applications*; Pergamon Press: New York, 1973. (b) Gates, B. C.; Katzer, J. R.; Schuit, G. C. A. *Chemistry of Catalytic Processes*; McGraw-Hill: New York, 1979. (c) Bogdanovich, B.; Göttsch, P.; Rubach, M. *J. Mol. Catal.* 1981, 11, 135.
- (5) (a) Tributsch, H. *Ber. Bunsen-Ges. Phys. Chem.* 1977, 81, 361; 1978, 82, 169. (b) Tributsch, H. *J. Electrochem. Soc.* 1978, 125, 169. (c) Tributsch, H. *J. Photochem.* 1985, 29, 89. (d) Tributsch, H. In *Modern Aspects of Electrochemistry*; Bockris, J. O. M.; Conway, B. E., White, R. E., Eds.; Plenum Press: New York, London, 1986; Vol. 17, p 303. (e) Alonso Vante, N.; Jaegermann, W.; Tributsch, H.; Hönl, W.; Yvon, K. *J. Am. Chem. Soc.* 1987, 109, 3251. (f) Ennaoui, A.; Fiechter, S.; Goslowsky, H.; Tributsch, H. *J. Electrochem. Soc.* 1985, 132, 1579.

<sup>†</sup> Liebig-Fellow (1986-1988).

<sup>‡</sup> Universität Münster.

<sup>§</sup> Cornell University.

<sup>||</sup> University of Hyderabad.